



## Topographic Representation of Numerosity in the Human Parietal Cortex

B. M. Harvey *et al.*

*Science* **341**, 1123 (2013);

DOI: 10.1126/science.1239052

*This copy is for your personal, non-commercial use only.*

If you wish to distribute this article to others, you can order high-quality copies for your colleagues, clients, or customers by [clicking here](#).

Permission to republish or repurpose articles or portions of articles can be obtained by following the guidelines [here](#).

**The following resources related to this article are available online at [www.sciencemag.org](http://www.sciencemag.org) (this information is current as of September 5, 2013):**

**Updated information and services**, including high-resolution figures, can be found in the online version of this article at:

<http://www.sciencemag.org/content/341/6150/1123.full.html>

**Supporting Online Material** can be found at:

<http://www.sciencemag.org/content/suppl/2013/09/04/341.6150.1123.DC1.html>

<http://www.sciencemag.org/content/suppl/2013/09/04/341.6150.1123.DC2.html>

A list of selected additional articles on the Science Web sites **related to this article** can be found at:

<http://www.sciencemag.org/content/341/6150/1123.full.html#related>

This article **cites 63 articles**, 26 of which can be accessed free:

<http://www.sciencemag.org/content/341/6150/1123.full.html#ref-list-1>

Robust increases in pERK occur in MSNs of the nucleus accumbens in response to psychostimulants and other drugs of abuse and are considered critical for enabling their long-lasting behavioral changes (22, 25, 26). The induction of such behaviors is inhibited by the local or systemic application of MAPK kinase (MEK) or ERK kinase inhibitors, such as SL327 (22, 27–29). To determine whether striatal ERK phosphorylation was necessary for the abnormal increase in locomotor activity, *Slc12a2<sup>K842\*/K842\*</sup>* mice were given an intraperitoneal injection or a local injection of SL327 to the nucleus accumbens. In both sets of experiments, SL327 administration restored locomotor activity to normal levels without affecting the levels of activity in controls (Fig. 4). Mutant mice treated with local SL327 returned to their baseline, presurgery locomotor levels of activity by day 3, which suggested that the injection did not cause permanent damage. SL327 administration did not affect grooming, which suggested that increased striatal pERK selectively elevates locomotor activity levels and not general activity.

This study demonstrates that inner ear dysfunction can induce molecular changes in the striatum that promote increased motor hyperactivity. The neural circuits linking inner ear defects to abnormal striatal function are likely transmitted by the normal auditory and vestibular input pathways, primarily via the thalamus and neocortex (30), but this remains to be demonstrated. Our results also suggest that a neurobiological cause, rather than simply socioenvironmental factors, contributes to the high incidence of behavioral disorders associated with inner ear dysfunction in

children and adolescents. Moreover, disruption of the ERK pathway in the striatum provides a potential target for intervention. Finally, it is intriguing to ponder whether sensory impairments other than those associated with inner ear defects could also cause or contribute to psychiatric or motor disorders that have traditionally been considered exclusively of cerebral origin.

#### References and Notes

- P. A. Selz, M. Girardi, H. R. Konrad, L. F. Hughes, *Otolaryngol. Head Neck Surg.* **115**, 70–77 (1996).
- S. L. Cushing, B. C. Papsin, J. A. Rutka, A. L. James, K. A. Gordon, *Laryngoscope* **118**, 1814–1823 (2008).
- P. Vostanis, M. Hayes, M. Du Feu, J. Warren, *Child Care Health Dev.* **23**, 233–246 (1997).
- P. Hindley, L. Kroll, *J. Deaf Stud. Deaf Educ.* **3**, 64–72 (1998).
- T. van Eldik, P. D. Treffers, J. W. Veerman, F. C. Verhulst, *Am. Ann. Deaf* **148**, 390–395 (2004).
- T. van Gent, A. W. Goedhart, P. A. Hindley, P. D. Treffers, *J. Child Psychol. Psychiatry* **48**, 950–958 (2007).
- L. Stiles, Y. Zheng, C. L. Darlington, P. F. Smith, *Behav. Brain Res.* **227**, 150–158 (2012).
- M. Schirmer *et al.*, *Brain Res.* **1155**, 179–195 (2007).
- F. M. Lambert, D. Combes, J. Simmers, H. Straka, *Curr. Biol.* **22**, 1649–1658 (2012).
- M. S. Deol, *J. Mol. Genet.* **5**, 137–158 (1968).
- J. J. Crouch, N. Sakaguchi, C. Lytle, B. A. Schulte, *J. Histochem. Cytochem.* **45**, 773–778 (1997).
- M. D. Plotkin, M. R. Kaplan, *et al.*, *Am. J. Physiol. Cell Physiol.* **272**, C173–C183 (1997).
- E. Delpire, J. Lu, R. England, C. Dull, T. Thorne, *Nat. Genet.* **22**, 192–195 (1999).
- M. J. Dixon *et al.*, *Hum. Mol. Genet.* **8**, 1579–1584 (1999).
- M. Flagella *et al.*, *J. Biol. Chem.* **274**, 26946–26955 (1999).
- A. J. Pace *et al.*, *J. Clin. Invest.* **105**, 441–450 (2000).
- R. J. Baldessarini, in *Goodman and Gilman's The Pharmacological Basis of Therapeutics*, L. L. Brunton, J. S. Lazo, K. Parker, I. Buxton, D. Blumenthal, Eds. (McGraw Hill, New York, ed. 11, 2006), pp. 317–399.

- N. C. Dubois, D. Hofmann, K. Kaloulis, J. M. Bishop, A. Trumpp, *Genesis* **44**, 355–360 (2006).
- J. A. Gorski *et al.*, *J. Neurosci.* **22**, 6309–6314 (2002).
- R. A. Kimmel *et al.*, *Genes Dev.* **14**, 1377–1389 (2000).
- J. Stenman, H. Toresson, K. Campbell, *J. Neurosci.* **23**, 167–174 (2003).
- E. Valjent *et al.*, *Proc. Natl. Acad. Sci. U.S.A.* **102**, 491–496 (2005).
- E. S. Choe, J. Q. Wang, *Neuroreport* **13**, 1013–1016 (2002).
- A. J. Silva, J. H. Kogan, P. W. Frankland, S. Kida, *Annu. Rev. Neurosci.* **21**, 127–148 (1998).
- T. V. Gerdjikov, G. M. Ross, R. J. Beninger, *Behav. Neurosci.* **118**, 740–750 (2004).
- J. Salzmann, C. Marie-Claire, S. Le Guen, B. P. Roques, F. Noble, *Br. J. Pharmacol.* **140**, 831–838 (2003).
- C. M. Atkins, J. C. Selcher, J. J. Petraitis, J. M. Trzaskos, J. D. Sweatt, *Nat. Neurosci.* **1**, 602–609 (1998).
- M. F. Favata *et al.*, *J. Biol. Chem.* **273**, 18623–18632 (1998).
- J. C. Selcher, C. M. Atkins, J. M. Trzaskos, R. Paylor, J. D. Sweatt, *Learn. Mem.* **6**, 478–490 (1999).
- T. Shiroyama, T. Kayahara, Y. Yasui, J. Nomura, K. Nakano, *J. Comp. Neurol.* **407**, 318–332 (1999).

**Acknowledgments:** We thank K. Khodakhah and P. Calderon for support with surgical approaches, rotarod, and early inputs to the project; G. Fishell for the Nestin-CreER mice in which *Slc12a2<sup>K842\*</sup>* arose; S. Zukin for Western blotting; C. Heinze for *Slc12a2<sup>flx</sup>* genotyping; University of California at Davis and NIH NeuroMab for antibodies; and the Developmental Studies Hybridoma Bank for the T4 antibody developed by Lytle and Forbush. This work was supported by the Tourette Syndrome Association (J.M.H. and K. Khodakhah), NIH R21NS073761 and R01MH083804 (J.H.), and Deutsche Forschungsgemeinschaft HU 800/5-1 (C.A.H.).

#### Supplemental Materials

www.sciencemag.org/cgi/content/full/341/6150/1120/DC1  
Materials and Methods

Figs. S1 to S5

Movies S1 and S2

References (31–40)

13 May 2013; accepted 8 August 2013

10.1126/science.1240405

## Topographic Representation of Numerosity in the Human Parietal Cortex

B. M. Harvey,<sup>1\*</sup> B. P. Klein,<sup>1</sup> N. Petridou,<sup>2</sup> S. O. Dumoulin<sup>1</sup>

Numerosity, the set size of a group of items, is processed by the association cortex, but certain aspects mirror the properties of primary senses. Sensory cortices contain topographic maps reflecting the structure of sensory organs. Are the cortical representation and processing of numerosity organized topographically, even though no sensory organ has a numerical structure? Using high-field functional magnetic resonance imaging (at a field strength of 7 teslas), we described neural populations tuned to small numerosities in the human parietal cortex. They are organized topographically, forming a numerosity map that is robust to changes in low-level stimulus features. The cortical surface area devoted to specific numerosities decreases with increasing numerosity, and the tuning width increases with preferred numerosity. These organizational properties extend topographic principles to the representation of higher-order abstract features in the association cortex.

Humans and many other animals use numerosity to guide behavior and decisions (1–4). Numerosity perception becomes less precise as the size of numbers increases (4–8) and is particularly effective for small numbers

(9). Animals, infants, and tribes with no numerical language perceive numerosity (1, 10–12), although they cannot count or use symbolic representations of number. Thus, numerosity processing is an evolutionarily preserved cognitive

function, distinct from counting and humans' unique symbolic and mathematical abilities (12). Because aspects of numerosity processing mirror primary sensory perception, it has been referred to as a “number sense” (2, 3).

The primary sensory and motor cortices in the brain are organized topographically. Is the neural organization for numerosity similarly topographic? The neural representation of numerosity resides in higher-order association cortices, including the posterior parietal cortex. Human functional magnetic resonance imaging (fMRI) consistently identifies this region as particularly responsive to numerosity manipulations (6, 12–14), and in similar regions, macaque neurophysiology describes neurons tuned to visual numerosity (4, 5, 7, 15). Both human fMRI and macaque neurophysiological response properties are closely linked to behavioral numerosity performance (4, 6).

We elicited responses to visual patterns with varying numerosity in study participants, while

<sup>1</sup>Department of Experimental Psychology, Helmholtz Institute, Utrecht University, Utrecht, 3584 CS, Netherlands. <sup>2</sup>Department of Radiology, Rudolf Magnus Institute of Neuroscience, University Medical Center Utrecht, Utrecht, 3584 CX, Netherlands.

\*Corresponding author. E-mail: b.m.harvey@uu.nl

**Fig. 1. Stimuli, responses, and neural population tuning.** (A) Illustration of stimulus conditions, with examples representing different numerosities. (B) Two example fMRI time courses from sites in the posterior parietal cortex, separated by about 2 cm, elicited by the numerosity stimulus sequence (top inset). BOLD, blood oxygen level–dependent. Points represent mean response amplitudes; error bars represent the standard error over repeated runs. In the upper panel, the largest response amplitude occurs after the presentation of low numerosities, whereas in the lower panel the largest response occurs with higher numerosities, considering the hemodynamic response delay. To quantify these differences, we developed a novel data-analysis method that extracts numerosity tuning from the time courses, following methods we developed in the visual cortex (17) (fig. S4). The numerosity model captures about 90% of the variance ( $R^2$ ) in the time courses, as indicated by the colored lines. (C) Representation of the neural model that best fits each time course. The model describes a Gaussian tuning function in logarithmic numerosity space with two parameters: preferred numerosity and tuning width defined by the full width at half maximum (FWHM). Different model parameters explain the differences seen in (B), capturing a similar amount of the variance.

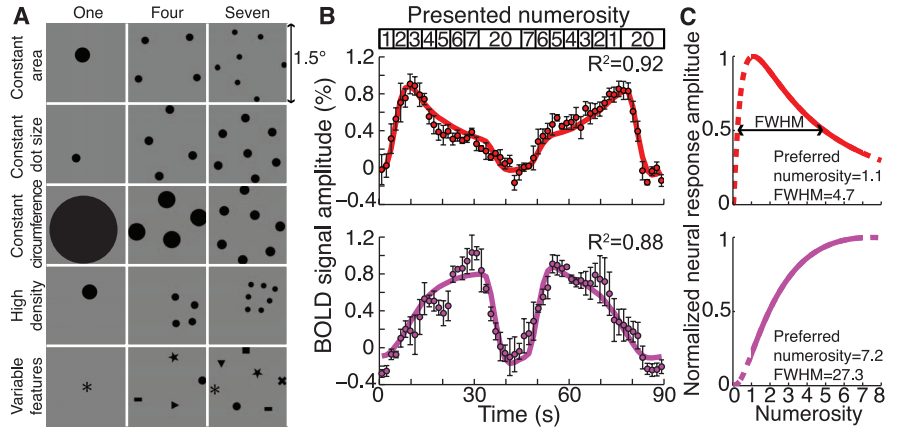
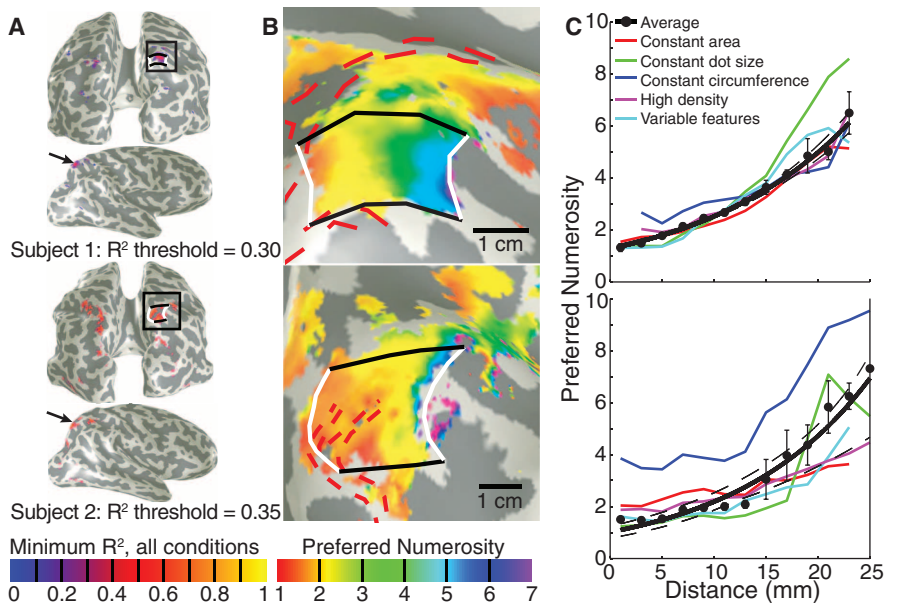


**Fig. 2. Topographic representation of numerosity.** (A) The variance explained by the model ( $R^2$ ) highlighted a region in the right parietal cortex where neural populations demonstrated numerosity tuning in all stimulus conditions (Fig. 1A). The black square is enlarged in (B). (B) Numerosity preferences for data averaged from all stimulus conditions, showing preferred numerosity increasing from the medial to lateral ends (white lines) of the region of interest (ROI) (black and white lines). Areas of low signal intensity, corresponding to pial surface veins (red dashed lines, fig. S3), were excluded from further analysis (30). (C) Numerosity preference progression from medial to lateral along the ROI for all conditions. All recording sites were organized by their distances from the two white lines. Dots represent the mean preferred numerosity in each distance bin, with error bars showing the standard error. We fitted the binned points with a logarithmic function (solid black line), with 95% confidence intervals to the fit (dashed black lines) determined by bootstrapping. More cortical area is devoted to lower number; i.e., cortical magnification decreases at higher numerosity. Different stimulus conditions are represented as colored lines joining the condition-specific bin means.



acquiring high-field (7 teslas) fMRI data. Changing numerosity in a visual display affects visual features such as luminance, contrast, density, and total edge length. Therefore, establishing numerosity selectivity requires several control conditions (Fig. 1A and figs. S1 and S2) (15). Consequently, we included conditions in which total dot area (“constant area” condition), individual dot size (“constant dot size”), or total dot circumference (“constant circumference”) were constant. A further condition contained much higher dot pattern density (“high density”). Finally, to check generalization to other objects, we replaced dots with different shapes (“variable features”). During stimulus presentation, participants reported when dots were shown in white rather than black (10% of presentations). No numerosity judgments were required. Participants performed above 90% correct.

The displayed numerosity varied systematically within an fMRI scan (Fig. 1B, top inset). This stimulus elicited remarkably different response profiles at different recording sites (Fig. 1B), despite having similar hemodynamic response functions (fig. S6). We summarized these fMRI signals using numerosity-tuned neural models (Fig. 1C and fig. S4). These describe Gaussian functions in logarithmic numerosity space, following behavioral (4), computational (16), neuroimaging (6), and neurophysiological (4, 5) results (fig. S5). The models have two parameters: preferred numerosity and tuning width (the numerosity range to which the population responds). This analysis is analogous to conventional population receptive field analysis in the visual cortex (17). These models explain much of the signal variance ( $R^2$ ), summarizing fMRI responses with two parameters. They capture similar amounts

of variance for both example response profiles in Fig. 1B, explaining time course differences by different numerosity tunings (Fig. 1C).

A specific region in the posterior parietal cortex was highlighted, where the models captured much response variance in all stimulus conditions (Fig. 2A and fig. S7). This region’s position was consistent between the eight participants, in the posterior superior parietal lobule, centered at mean (SD) Montreal Neurological Institute  $x,y,z$  coordinates of 23 (4),  $-60$  (7),  $60$  (7) (18) and closely matches previous reports of a region responding strongly to numerosity manipulations (6, 12–14).

Projecting each recording site’s preferred numerosity onto the unfolded cortical surface revealed an orderly topographic map (Fig. 2B). Medial and lateral regions preferred low and high numerosities, respectively. The topographic

**Fig. 3. Comparison of numerosity preferences across recording points in different stimulus conditions, averaged across participants.** (A) Because numerosity preferences are topographically organized in all stimulus conditions, they are always correlated. (B) However, preferences change with stimulus conditions, with preference increasing particularly in the constant circumference condition.  $t$ ,  $t$  statistic.

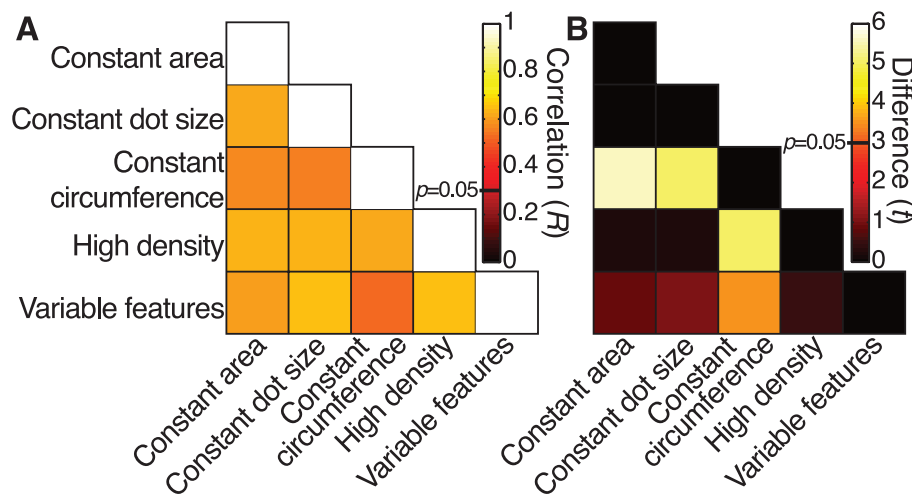
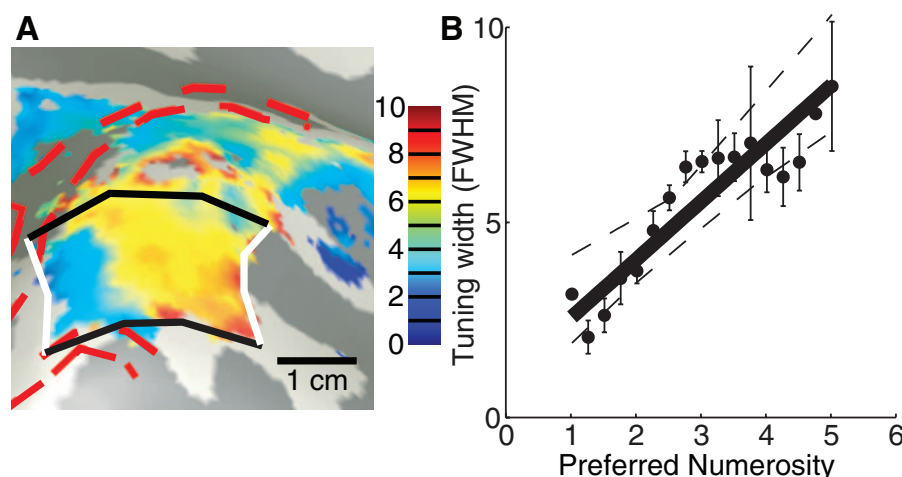


**Fig. 4. The progression of population tuning width (see Fig. 1C) across the cortical surface (A) and with preferred numerosity (B) for one representative participant.** Dots represent mean tuning widths in each preferred numerosity bin, and error bars represent standard errors. Dashed lines represent 95% confidence intervals of the fit (solid line) to the bin means. Tuning width increases with preferred numerosity for all participants (fig. S13B).



progression and its direction were consistent between participants and stimulus conditions (fig. S8). Numerosity selectivity was also present in the left hemisphere (fig. S9) and in neighboring regions of the right hemisphere, but with lower variance explained and less clear, less consistent topographic structure. To quantify the numerosity organization, we sorted recording sites within this region by their distance from the borders representing lowest and highest numerosities (white lines in Fig. 2B). We then plotted preferred numerosity against cortical distance for individual stimulus conditions and their average (Fig. 2C and fig. S10).

Numerosity preference was organized topographically in all stimulus conditions, so numerosity preference is significantly correlated between conditions (Fig. 3A and fig. S11A). However, absolute numerosity preference varied with stimulus condition (Fig. 3B and fig. S11B), which is consistent with results from single macaque neurons (5). In particular, the constant circumference condition differs from other conditions. It has very different dot sizes from other conditions (Fig. 1A and fig. S2), and we propose that dot size interacts with numerosity preference, be-

cause line length–selective neurons are found with numerosity-selective neurons in the macaque posterior parietal lobe (19).

The rate of numerosity preference change with distance increased with numerosity; i.e., the cortical magnification factor decreases (Fig. 2C). Thus, more cortical surface area represents lower than higher numerosities (fig. S12). Similarly, more macaque posterior parietal neurons prefer low than high numerosities (5). Such over-represented parts of other topographic maps also show more precise response selectivity than elsewhere in the map; i.e., tuning width is smaller. Tuning widths changed across the topographic map along with preferred numerosity (Fig. 4A and fig. S13A). Population tuning width increased with preferred numerosity (Fig. 4B and fig. S13B), in line with single macaque neuron (4, 5), neuroimaging (6), and behavioral results (6–8). However, population tuning widths are larger than macaque single-neuron tuning widths (fig. S14). This may arise from differences in neural population size (~400,000 neurons in our recording points), the scatter of response preferences at a single cortical location, hemodynamic properties, interpolation steps in fMRI

analyses, task differences, and/or species differences (17).

Neuroimaging studies consistently show that this part of the parietal cortex responds to numerosity manipulations (6, 12–14), and parietal lesions can cause number-processing deficits (20). Macaque neurophysiology demonstrates numerosity tuning in single neurons in a similar parietal region (5), and human neural adaptation properties suggest that numerosity-tuned populations exist in the same area, with tuning widths increasing with preferred numerosity (6). We extended these observations by directly measuring numerosity tuning in the human cortex and describing a topographic organization of numerosity, a numerosity cortical magnification factor, and a relationship between preferred numerosity and numerosity tuning width. Based on similar behavioral performance and cortical location of numerosity-selective populations in humans and macaques, we expect similar topographic organization in macaques. The spatial scale of the topographic organization is several centimeters. Consequently, methodological limitations of single-neuron recordings may have prevented its identification; i.e., at single-neuron resolution, topography may

be obscured by the scatter of response properties, broad single-neuron tuning, neurons with other response properties, and an unknown direction of topography change. However, both methodologies are complementary, and our measurements are consistent with neurophysiology. Both support numerosity tuning, albeit at different scales, in similar parts of the brain, with more neurons tuned to smaller numerosities and increases in tuning width with preferred numerosity. These properties are analogous to organization properties of the sensory and motor cortices and may underlie the decreased precision at higher numerosities that is commonly seen in human and animal behavior (4, 6, 8, 12–14).

Our numerosity-selective responses cannot be explained by other visual attributes of the stimulus. First, tuning and topographic structure were found using stimuli controlled for low-level features. Second, responses in visual field maps such as V1 cannot be captured by the numerosity model but follow stimulus contrast energy (fig. S15). Third, parietal visual field map borders (21) did not correspond to numerosity map borders and their relative positions varied considerably between participants (fig. S16). In macaques, over 80% of single neurons here show no numerosity selectivity (5, 19), so independent representations of numerosity and visual space may exist in one cortical region, represented by different neurons. Alternatively, these populations have large visual receptive fields and may be tuned to numerosity presented anywhere within this receptive field. Interactions between overlapping numerosity and visuospatial representations may underlie the cognitive spatial “number line” (11, 22). However, we find no consistent relationship between numerosity and visuospatial responses.

What is the nature of the numerosity representation? We found no number-tuned responses for Arabic numerals (fig. S17), suggesting that neurons here do not respond to symbolic number representations. We propose that current biologically plausible computational models of numerosity processing, driven by visual features, can produce the numerosity selectivity we see (16, 23). Some models suggest that (as we find) numerosity selectivity depends on stimulus features, such as dot size (23). Computational models of nu-

merosity extraction may thus explain these differences in numerosity tuning, consistent with behavioral results (7, 23).

Numerosity processing and its cortical organization may be fundamental to human abilities in mathematics and economics. Although numerosity judgments and complex mathematical abilities rely on different processes, individual differences in these abilities are correlated (24). Macaques and young children can perform simple, approximate addition and subtraction (25, 26). In macaques, the parietal and prefrontal cortices contain neurons responding specifically during simple mathematical tasks, together with numerosity-selective neurons (27). Associations between visual numerosity and symbolic number representations develop early in life (10). Numerosity, number, and size are fundamental to our understanding of magnitude and quantity and underlie higher-level concepts of value (22).

Our results demonstrate that topographic representations, common in the sensory and motor cortices, can emerge within the brain to represent abstract features such as numerosity. Similarities in cortical organization suggest that the computational benefits of topographic representations, for example efficiency in wiring (28, 29), apply to higher-order cognitive functions and sensory-motor functions alike. As such, topographic organization may be common in higher cognitive functions. On the other hand, topographic organization supports the view that numerosity perception resembles a primary sense (2, 3). These views are not mutually exclusive, but both challenge the established distinction between primary topographic representations and abstracted representations of higher cognitive functions.

#### References and Notes

1. E. M. Brannon, H. S. Terrace, *Science* **282**, 746–749 (1998).
2. D. Burr, J. Ross, *Curr. Biol.* **18**, 425–428 (2008).
3. S. Dehaene, *The Number Sense: How the Mind Creates Mathematics* (Oxford Univ. Press, New York, 1997).
4. A. Nieder, E. K. Miller, *Neuron* **37**, 149–157 (2003).
5. A. Nieder, E. K. Miller, *Proc. Natl. Acad. Sci. U.S.A.* **101**, 7457–7462 (2004).
6. M. Piazza, V. Izard, P. Pinel, D. Le Bihan, S. Dehaene, *Neuron* **44**, 547–555 (2004).
7. M. Tokita, A. Ishiguchi, *Atten. Percept. Psychophys.* **72**, 1839–1853 (2010).

8. J. Whalen, C. R. Gallistel, R. Gelman, *Psychol. Sci.* **10**, 130–137 (1999).
9. I. J. Saltzman, W. R. Garner, *J. Psychol.* **25**, 227–241 (1948).
10. J. F. Cantlon *et al.*, *J. Cogn. Neurosci.* **21**, 2217–2229 (2009).
11. S. Dehaene, V. Izard, E. Spelke, P. Pica, *Science* **320**, 1217–1220 (2008).
12. S. Dehaene, E. Spelke, P. Pinel, R. Stanescu, S. Tsivkin, *Science* **284**, 970–974 (1999).
13. E. Eger *et al.*, *Curr. Biol.* **19**, 1608–1615 (2009).
14. P. Pinel *et al.*, *Neuroreport* **10**, 1473–1479 (1999).
15. A. Nieder, D. J. Freedman, E. K. Miller, *Science* **297**, 1708–1711 (2002).
16. S. Dehaene, J. P. Changeux, *J. Cogn. Neurosci.* **5**, 390–407 (1993).
17. S. O. Dumoulin, B. A. Wandell, *Neuroimage* **39**, 647–660 (2008).
18. D. L. Collins, P. Neelin, T. M. Peters, A. C. Evans, *J. Comput. Assist. Tomogr.* **18**, 192–205 (1994).
19. O. Tudusciuc, A. Nieder, *Proc. Natl. Acad. Sci. U.S.A.* **104**, 14513–14518 (2007).
20. S. Dehaene, L. Cohen, *Neuropsychologia* **29**, 1045–1074 (1991).
21. J. D. Swisher, M. A. Halko, L. B. Merabet, S. A. McMains, D. C. Somers, *J. Neurosci.* **27**, 5326–5337 (2007).
22. V. Walsh, *Trends Cogn. Sci.* **7**, 483–488 (2003).
23. S. C. Dakin, M. S. Tibber, J. A. Greenwood, F. A. Kingdom, M. J. Morgan, *Proc. Natl. Acad. Sci. U.S.A.* **108**, 19552–19557 (2011).
24. J. Halberda, M. M. Mazocco, L. Feigenson, *Nature* **455**, 665–668 (2008).
25. J. F. Cantlon, E. M. Brannon, *PLoS Biol.* **5**, e328 (2007).
26. P. Starkey, *Cognition* **43**, 93–126 (1992).
27. S. Bongard, A. Nieder, *Proc. Natl. Acad. Sci. U.S.A.* **107**, 2277–2282 (2010).
28. B. L. Chen, D. H. Hall, D. B. Chklovskii, *Proc. Natl. Acad. Sci. U.S.A.* **103**, 4723–4728 (2006).
29. S. Ramón y Cajal, P. Pasik, T. Pasik, *Texture of the Nervous System of Man and the Vertebrates* (Springer, New York, 1999).
30. J. Winawer, H. Horiguchi, R. A. Sayres, K. Amano, B. A. Wandell, *J. Vis.* **10**, 1 (2010).

**Acknowledgments:** Processed data reported in the paper are presented in full in the supplementary materials. Raw data and custom analysis code are available on request from the authors. This work was supported by Nederlandse Organisatie voor Wetenschappelijk Onderzoek Vidi grant 452.08.008. We thank J. W. Brascamp for critical comments on the manuscript.

#### Supplementary Materials

www.sciencemag.org/cgi/content/full/341/6150/1123/DC1  
Materials and Methods  
Figs. S1 to S17  
References (31–65)

11 April 2013; accepted 8 August 2013  
10.1126/science.1239052